Conference paper

Zhen Luo[a], Jun Chen[a], Qingchen Shen, Jiaqing He, Hao Shan, Chengyi Song, Peng Tao, Tao Deng* and Wen Shang*

Bioinspired infrared detection using thermoresponsive hydrogel nanoparticles

DOI 10.1515/pac-2015-0101

Abstract: The development of high performance uncooled infrared (IR) detection and imaging systems will greatly expand the application of IR technology in broad areas such as transportation, environmental monitoring, and medical care. Inspired by the superior IR detection capability of beetle *Melanophila acuminata*, we explored the potential use of hydrogel nanoparticles (NPs) in uncooled IR detection system. In the system, the absorption of the incoming IR radiation by the temperature-sensitive hydrogel NPs, together with water, induces the volume change of the hydrogel NPs, similar to the volume change of the biofluid inside the sensillae receptors in *M. acuminata* caused by the IR radiation. This volume change results in the change of optical readout (transmittance in this study) in visible range and provides the sensitive detection of the IR radiation. In this work, poly(N-isopropylacrylamide-co-acrylic acid) (poly(NIPAM-*co*-AAc)) copolymer NPs with different sizes were synthesized and their IR sensing performances were studied in detail. The correlation between the NP size and concentration and the IR sensing property was also discussed in the paper. This work helps enhance the understanding of the response of hydrogel NPs under IR radiation, and offers a potential material system for uncooled IR detection that is inspired by *M. acuminata*. The direct use of transmittance of the NP solution as the readout for IR detection also provides a simple and sensitive IR detection approach for low cost and portable industrial applications.

Keywords: absorption; bioinspired; hydrogel; infrared; nanoparticles; NICE-2014; thermoresponsive.

Introduction

Infrared (IR) detectors are widely used in many important applications, which include thermal imaging, military tracking, and alarm systems. Cooled IR detectors, such as HgCdTe detectors, usually have high sensitivity but also are relatively expensive due to the extra cooling requirement. Uncooled IR detectors, such as thermo-mechanical IR detectors, avoid the need of cooling but involve complex structures and the associated

Article note: A collection of invited papers based on presentations at the 2nd International Conference on Bioinspired and Biobased Chemistry and Materials: Nature Inspires Chemical Engineers (NICE-2014), Nice, France, 15–17 October 2014.

[a]Zhen Luo and Jun Chen contributed equally to this work.

***Corresponding authors: Tao Deng and Wen Shang,** State Key Laboratory of Metal Matrix Composites, Shanghai Jiao Tong University, Shanghai 200240, People's Republic of China; and School of Materials Science and Engineering, Shanghai Jiao Tong University, Shanghai 200240, People's Republic of China, e-mail: dengtao@sjtu.edu.cn (T. Deng), shangwen@sjtu.edu.cn (W. Shang)

Zhen Luo, Jun Chen, Qingchen Shen, Jiaqing He, Hao Shan, Chengyi Song and Peng Tao: State Key Laboratory of Metal Matrix Composites, Shanghai Jiao Tong University, Shanghai 200240, People's Republic of China; and School of Materials Science and Engineering, Shanghai Jiao Tong University, Shanghai 200240, People's Republic of China

complicated fabrication processes [1–3]. Developing highly sensitive and low cost uncooled IR detection materials and systems is one of the current driving forces for the further development of IR technology. Recently, using bio-inspired approach to develop high performance IR sensing systems has attracted much attention [4–10]. Some natural biological species, such as fire beetles [11, 12], and snakes [13], have outstanding capability to detect IR radiation. Among them, the *M. acuminata* beetles have the most fascinating IR detection ability to detect forest fire even from the distance as far as 60–100 miles away. These beetles have IR detection organs located behind their middle legs on both sides, and each IR detection organ contains ~70 IR receptors (sensilla) with size of ~12–15 μm. The superior IR detection capability of these beetles relies on the photomechanical principle: under the IR radiation, the fluid inside the IR receptors of the beetle absorbs the IR energy, changes the volume, and induces a series of physical and biological responses. The incoming IR signal can be transferred and detected by the mechano-sensitive neuron of the beetle (Fig. 1a) [5, 11, 12].

Inspired by the IR detection mechanism of beetle *M. acuminata*, in this paper, we explored the potential use of poly(N-isopropylacrylamide) (PNIPAM)-based thermal sensitive hydrogel copolymer nanoparticles (NPs), which also change volume upon heating or cooling, for the uncooled IR detection. Thermo-sensitive hydrogels have been used in a broad range of applications including filtration membranes [14], drug-release microcapsules [15], sensors and actuators, etc. [16, 17]. For the thermal sensitive hydrogel NPs, when the temperature is below the lower critical solubility temperature (LCST), the NPs are hydrophilic and in swollen state. When the temperature increases, the hydrogel NPs lose water and their volume decreases. As the temperature reaches to above LCST, the hydrogel NPs become hydrophobic and change to collapsed state. Such temperature dependent volume change of hydrogel NPs has been reported for potential temperature sensing application, in which the NPs formed an ordered crystalline colloidal array (CCA) and were fixed by a polymer matrix as a polymerized crystalline colloidal array (PCCA). The diffraction peak intensity of PCCA is highly temperature dependent and such PCCA system can be used as temperature sensor, as reported by Asher's group [18]. Based on such phenomenon, we hypothesize that the temperature sensitive hydrogel NPs should also be highly sensitive to IR radiation, since IR radiation will induce the temperature change of the system and result in optical property changes of the NP system. Figure 1 shows the schematic of IR detection approach using thermo-sensitive hydrogel NPs. Similar to the volume change of the biofluid inside the sensillae receptors of *M. acuminata* (Fig. 1a) [19, 20], there is also a volume change of hydrogel NPs upon IR radiation. As the

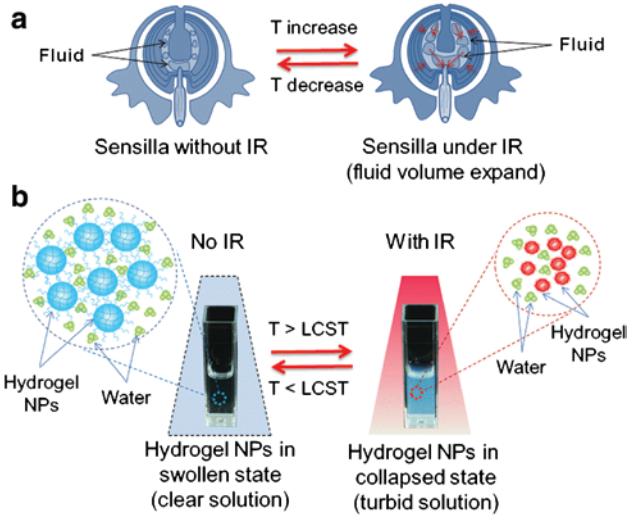

Fig. 1: Schematic of the IR detection principle using thermo-responsive hydrogel NPs that were inspired by *Melanophila Acuminata* beetle. (a) The IR detection principle of the sensilla of beetle: the fluid volume changes (expanding) under IR illumination and such volume change generates a neuron signal; (label the expansion in the figure). (b) The IR detection principle of the hydrogel NPs: the NP volume changes (shrinking) under IR illumination and such volume change generates an optical signal (changes in turbidity).

hydrogel NP system absorbs the IR radiation, the temperature of the NP system rises, and hydrogel NPs loose water and shrink to collapsed state. Due to the refractive index change of the hydrogel NPs from swollen state to collapsed state, the NP solution changes from a clear state (swollen state) to a turbid state (collapsed state), which results in the sensitive change in the optical transmission of the hydrogel NP solution. In this study, the change of transmission of randomly dispersed hydrogel NP solution upon IR radiation was monitored and used as the optical readout. Poly(N-isopropylacrylamide-*co*-acrylic acid) (poly(NIPAM-*co*-AAc)) hydrogel NPs with different sizes were synthesized and their sensitivity to IR radiation was investigated. Both the size and the concentration of hydrogel NPs affect the IR sensing property of the detection system, with the size effect is more dramatic than the concentration effect. This study demonstrates that the thermo-sensitive hydrogel NPs can be used as a sensitive system for the uncooled IR detection.

Results and discussion

Synthesis and characterization of poly(NIPAM-*co*-AAc) NPs

The detailed information for the synthesis of poly(NIPAM-*co*-AAc) hydrogel NPs are given in Table S1. The synthesis follows a typical free radical emulsion polymerization process [18]. The amounts of chemical used were varied in order to get the NPs with different sizes.

The fourier transform infrared spectroscopy spectra (Fig. S1) confirm that the PNIPAM hydrogel consists of hydrophilic group of acylamino (–CONH–) and hydrophobic group of isopropyl (–CH $(CH_3)_2$). The spectra also confirm the existence of carboxylate (–COOH) group.

Analysis of the poly(NIPAM-*co*-AAc) hydrogel NPs by SEM (Fig. 2a–c) revealed that the hydrogel NPs synthesized in this work were relatively uniform in size. The decreasing of sodium dodecyl sulfate (SDS) concentration during synthesis generated hydrogel NPs with increased sizes. The conformation and size of the hydrogel NPs were further characterized using AFM. Figure 2d–f provide the AFM micrographs of three different poly(NIPAM-*co*-AAc) NPs together with the line scan profiles. The AFM images show that the NPs on the surface are not spherical but rather deformed, which may be caused by the drying and spin-coating processes. The sizes of the hydrogel NPs were calculated based on the assumption that the volumes of the hemisphere NPs on the Si wafer surface are the same as the spherical NPs in hydrophobic state in solution (supporting info). The diameters of the three NP samples were thus calculated to be ~120 nm, ~170 nm, and ~300 nm.

The DSC analysis for hydrogel NPs are shown in Fig. 3. The endothermic peaks are at 31.9 °C for 120-nm NP sample, 30.9 °C for 170-nm NP sample, and 30.3 °C for 300-nm sample, respectively. These peaks also correspond to the LCST data of each sample. The results indicated that the LCST of hydrogel NPs slightly decreases when NP size increases. We hypothesis that such slight increase of LCST with smaller NPs may be due to the higher degree of surface and volume confinement for smaller NPs than those for larger NPs.

The IR response of poly(NIPAM-*co*-AAc) NPs with different sizes

At temperature below LCST, the functional group of acylamido on the chain of pNIPAM combines with water and forms a six-member ring structure through hydrogen bonds and the hydrogel NPs are in swollen state. The hydrogel NPs at the swollen state are hydrophilic so the solution is clear. When the hydrogel is heated, the hydrogen bonds between acylamido and water become weak and the hydrogel loses water severely at temperature around LCST. The acylamido will then combine together by intramolecular hydrogen bonds. This intra-molecular bonding leads to the decrease of molecular spacing and the shrinking of hydrogel volume. The hydrogel NPs then change from the swollen state to the collapsed state [21]. As the hydrogel NPs loose water, they become hydrophobic, the refractive index of the NP increases, and such increase results in the rise of solution turbidity [22]. The transmittance of the NP solution therefore decreases correspondingly.

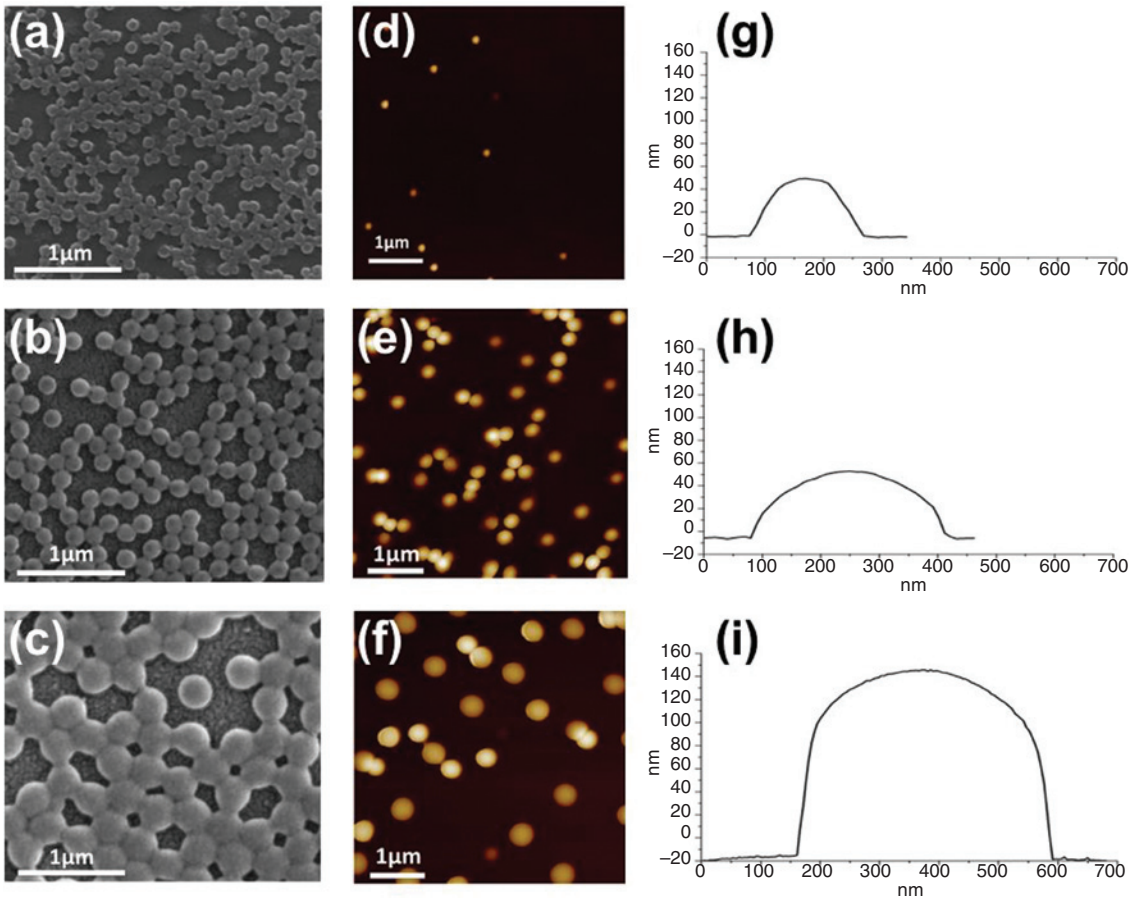

Fig. 2: The SEM and AFM characterization of poly(NIPAM-*co*-AAc) NPs. (a–c) SEM images of hydrogel NPs; (d–f) AFM analysis of hydrogel NPs; (g–i) AFM line scan profiles of single particles.

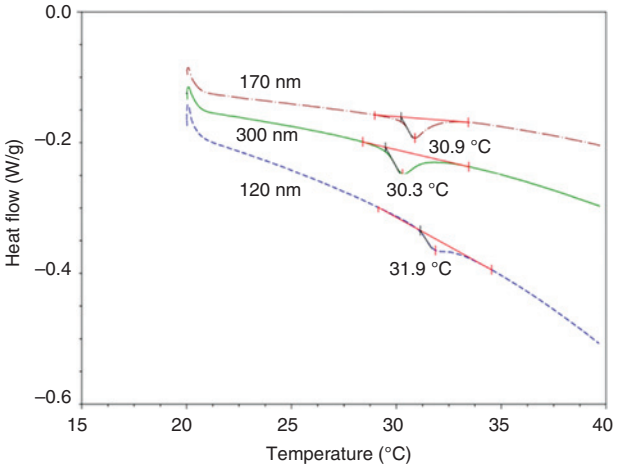

Fig. 3: DSC analysis for poly(NIPAM-*co*-AAc) hydrogel NPs with different sizes.

By monitoring the change of transmittance of those NP solution samples, the intensity of IR radiation can be measured.

Figure 4a shows the transmission spectra for the NP samples that have same solid contents (0.09 %) but different sizes. As the size of hydrogel NPs increases, the transmittance of the NP solution decreases, with

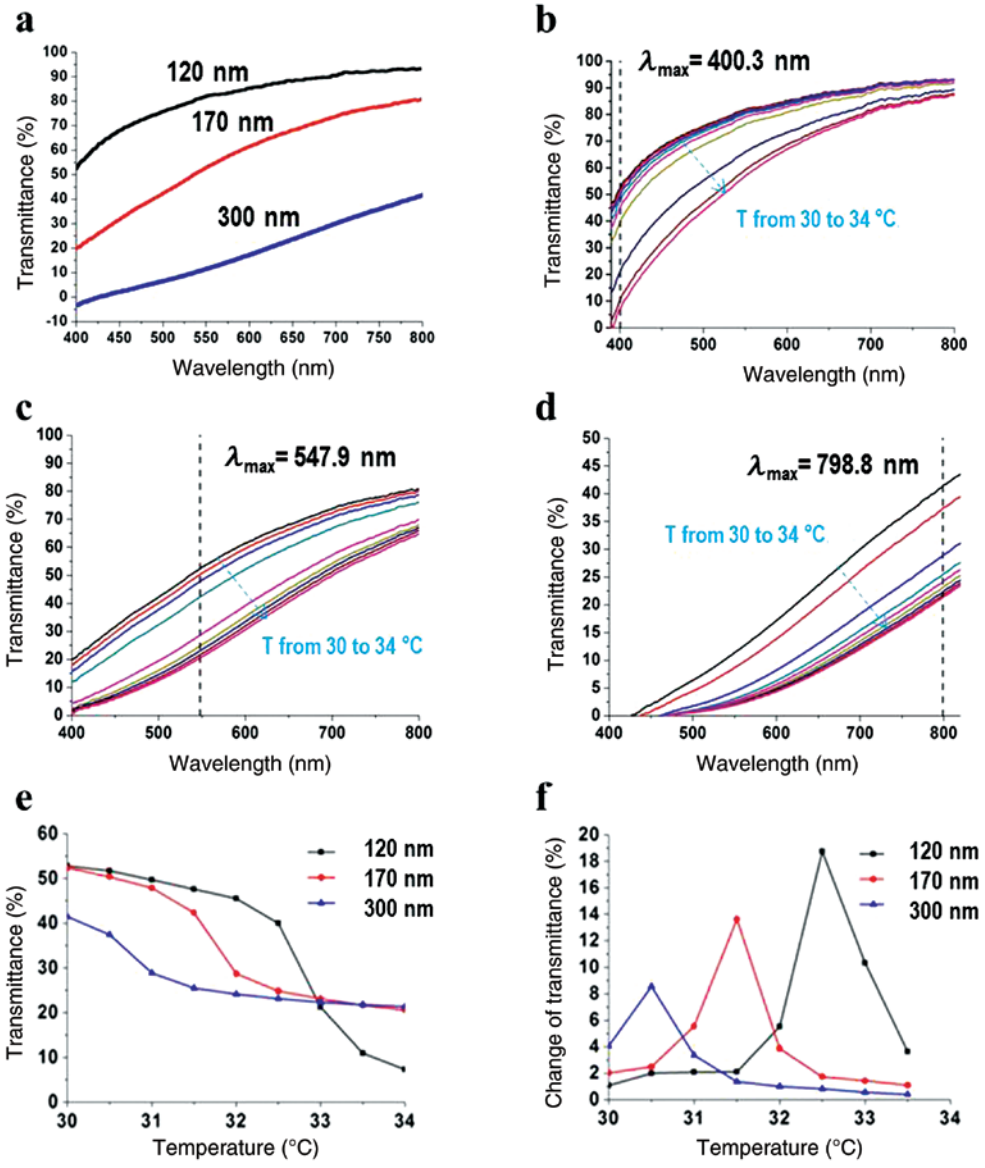

Fig. 4: IR radiation induced-temperature effects on transmittance for hydrogel NPs with different sizes. (a) The transmission spectra of NPs with sizes of 120, 170, and 300 nm before IR radiation. (b–d) The transmittance spectra upon IR radiation. (e) The transmittance and (f) the change of transmittance at λ_{max} with change of temperatures for different hydrogel NPs.

the 120-nm NP sample shows the highest transmittance. Large NPs usually have increased scattering effect [18] and hence the decreased transmittance. As shown in Fig. 4b–d, upon exposure to IR radiation, the temperature of the hydrogel NP solution increases, the hydrogel NPs loose water, and the transmittance of each sample decreases correspondingly. The small negative transmittance at shorter wavelength for the samples with larger turbidity was due to the dark baseline error from the open optical measurement system, which was used to accommodate the IR illumination and the temperature measurement. To obtain the change of transmittance with the change of temperature, Eq. 1 was used to calculate the change of the transmittance across the whole spectrum with each 0.5 °C temperature increase.

$$\Delta T_{tr}(T) = T_{tr}(T) - T_{tr}(T + 0.5) \tag{1}$$

Where $\Delta T_{tr}(T)$ is the change of transmittance from temperature T to (T + 0.5). $T_{tr}(T)$ is the transmittance at the temperature of T and $T_{tr}(T + 0.5)$ is the transmittance at the temperature of (T + 0.5). The calculated $\Delta T_{tr}(T)$ were plotted in Fig. S2.

The wavelengths with the most change of transmission (λ_{max}) were also marked in Fig. 4b–d. As the size of hydrogel NP increases, the λ_{max} increases. The λ_{max} is 400.3 nm for 120-nm NPs, 547.9 nm for 170-nm NPs, and 798.8 nm for 300-nm NPs. Such red-shift of λ_{max} may be due to the enhanced scattering effect of hydrogel NPs at large sizes.

The transmittance and the change of transmittance at λ_{max} with temperature for each NP sample were further plotted in Fig. 4e and f. As the temperature increased, the transmittance decreased gradually and the change of transmittance was relatively small. As the temperature reached close to LSCT, the hydrogel NPs collapsed, and included a sudden jump of refractive index of the hydrogel NPs. Such jump resulted in the largest decrease of the transmittance.

The 120-nm NP sample showed the highest transmittance change at 32.5 °C and NP samples with sizes of 170 nm and 300 nm showed the largest transmittance change at 31.5 °C and 30.5 °C, respectively. As the size of the NPs increases, the phase transition temperature slightly decreases, which is consistent with the LCST data measured by DSC. The slight difference in the LSCT between DSC and transmittance measurements might be due to the difference in temperature calibration between the two measurement systems.

The temperature sensitivity (TS) of poly(NIPAM-*co*-AAc) NPs was calculated using Eq. 2 [9]:

$$TS = N_{rms} / SITF_{slope} = N_{rms}\Delta T / \Delta(\Delta T_{tr}) \quad (2)$$

where N_{rms} is root mean square (r.m.s.) noise, SITF is the system intensity transfer function. Here $SITF_{slope} = \Delta(\Delta T_{tr})/\Delta T$, ΔT is the target-to-background differential temperature (here $\Delta T = 0.5$ K) and $\Delta(\Delta T_{tr})$ is the measured device response corresponding to temperature change of ΔT.

N_{rms} was measured to be 0.5 % for the hydrogel NP system, and the temperature sensitivities were calculated to be 29 mK, 42 mK and 100 mK for 120-nm, 170-nm, and 300-nm hydrogel NP samples, respectively, at their corresponding LSCT temperatures. The smallest hydrogel NP sample exhibited the highest temperature sensitivity. With the increase of hydrogel NP size, the TS decreases, as well as the IR sensitivity. The TS depends on the sensitivity of the change in the refractive index of the hydrogel NPs. Such change in the refractive index relies on the change of the NP states before and after IR radiation. Smaller NPs have shorter diffusion lengths than the larger NPs, which might lead to a faster and easier transport of water in and out of NPs and results in a more sensitive change in refractive index and a higher TS than those of larger NPs.

IR response of poly(NIPAM-*co*-AAc) NPs with different concentrations

Next the concentration effect on the IR response was studied for the 120-nm NPs, which showed the best TS among samples with different sizes. The 120-nm NP sample was adjusted with distilled water to have solid contents of 0.09 %, 0.30 %, 0.45 %, 0.60 %, and 0.90 %. The transmission responses to IR radiation were studied and discussed below.

Figure 5a gives the transmittance spectra for the 120-nm NP samples that have different solid contents, at temperature of 30 °C without IR radiation. As the concentration of hydrogel NPs increases, the transmittance of the NP solution decreases. NP sample with larger concentration has stronger scattering effect so that its light transmission is lower. Figure 5 (b–f) provide the transmittance spectra for 120-nm NP samples with different concentrations at different temperatures under IR radiation. As the concentration of hydrogel NPs becomes larger, the λ_{max} becomes red-shifted. This shift might also be attributed to the enhanced light scattering effect of hydrogel NPs at larger concentration.

Figure 5g and h show the transmittance and the change of transmittance at the λ_{max}. The maximum temperature sensitivities of these samples are calculated to be 29 mK, 56 mK, 56 mK, 63 mK, and 56 mK for NPs with solid contents of 0.09 %, 0.30 %, 0.45 %, 0.60 %, and 0.90 %, respectively. The sample with smallest concentration has the best temperature sensitivity. The sensitivity dropped when the NP concentration

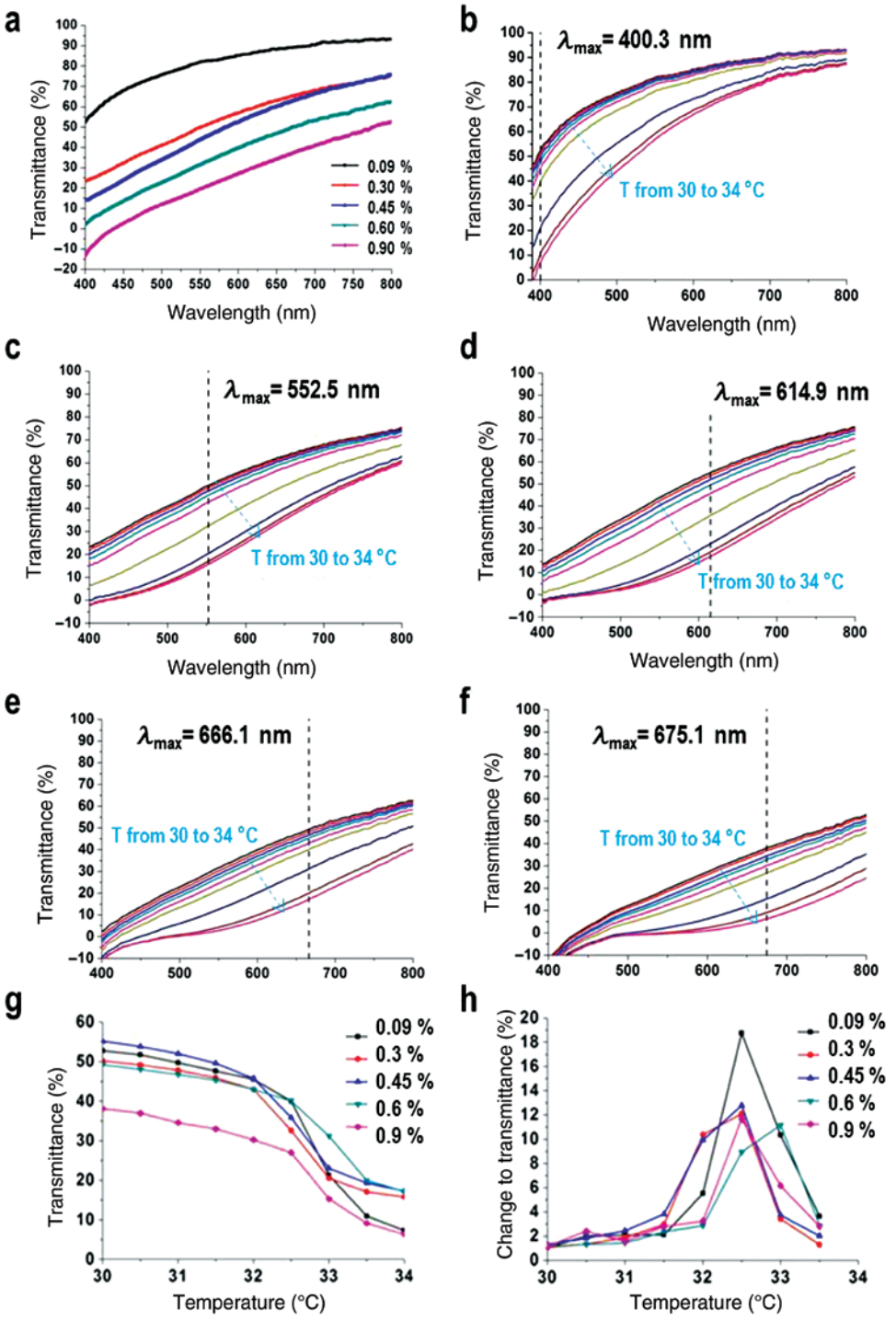

Fig. 5: (a) The transmission spectra of 120-nm hydrogel NP sample with different concentrations; (b–f) the wavelength dependence of sensitivity of transmittance spectra for the samples with different concentrations after IR radiation; the temperature dependence of transmittance (g) and the change of transmittance (h) of those samples at λ_{max}.

increases but further increasing of the NP concentration does not cause much change of the temperature sensitivity. Compared to Fig. 4, Fig. 5h shows that there is less a dependence of TS to the concentrations of NP solution than the dependence of TS to the sizes of the NPs.

Compared with natural IR detection system in *M. acuminata* beetles, which showed the temperature sensitivity (e.g. IR sensitivity) of 10 mK [20], our hydrogel NP system showed a comparable temperature

sensitivity of 29 mK. With further optimization of NPs, the artificial system should achieve similar or even better IR sensing performance as what natural system provides.

Dynamic response of hydrogel NP samples under modulated IR radiation

To investigate the response speed of poly(NIPAM-*co*-AAc) hydrogel NPs to the IR radiation, we measured the change of transmittance for 120-nm hydrogel NPs with solid content of 0.09 % under the periodic IR radiation using an optical chopper. The relative transmittance $T_{tr}^{R}(\lambda)$ of the IR responses were calculated using Eq. (3) [23]:

$$T_{tr}^{R}(\lambda) = 100\% \times [T_{tr}(\lambda)/T_{tr_0}(\lambda)] \tag{3}$$

where $T_{tr_0}(\lambda)$ is the transmittance of poly(NIPAM-*co*-AAc) NPs before IR radiation and $T_{tr}(\lambda)$ is a transmittance during IR exposure.

Figure 6 shows the dynamic response of the poly(NIPAM-*co*-AAc) NPs to the incoming IR radiation with a 0.02 Hz modulation frequency. The relatively slow response speed of hydrogel NPs can be attributed to two possible effects: (1) samples with a relatively large volume (1 mL) and relatively large optical path length (1 cm) were used in this study. Such large volume and optical path length generated large thermal mass and slow response; (2) The current water-based hydrogel sensing system has relatively low thermal conductivity that leads to poor heat dissipation during detection process. Decrease of the sample volume and increase of the heat dissipation should help speed up the IR response. Further study is currently underway to improve the IR response speed of the hydrogel-NP based IR detection system.

Conclusions

This work demonstrated a hydrogel NP based system for sensitive uncooled IR detection. A series of poly(NIPAM-*co*-AAc) hydrogel copolymer NPs with different sizes and concentrations were prepared and characterized in this study. The response of these hydrogel NPs to IR radiation were investigated in details through transmission spectra analysis. A temperature sensitivity of ~29 mK was achieved through the use of the hydrogel copolymer NPs with size of 120-nm. The findings in this paper indicated that the NP size has a more profound effect on the IR sensitivity than that of the NP concentrations. Small NPs have better IR sensitivity than large NPs. This study not only provides new insights of the response of hydrogel NPs to the IR radiation, but also offers a bioinspired approach for uncooled IR detection. The straightforward use of transmittance as the detection readout also enables the rapid implement of this system in low cost and portable commercial applications for IR imaging and IR detection.

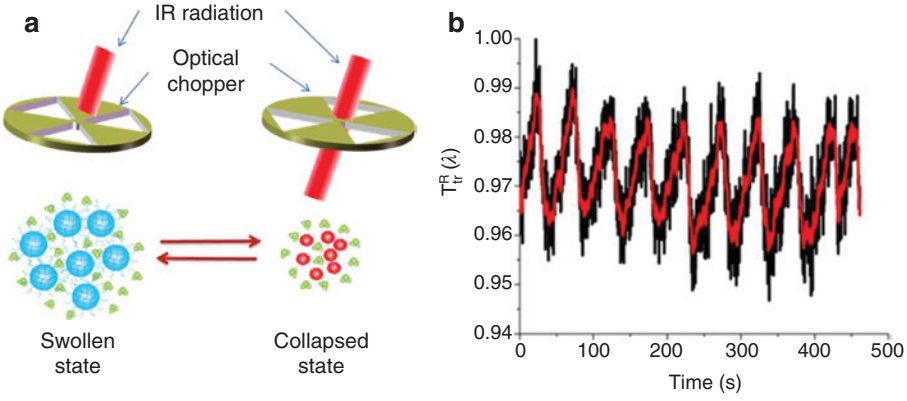

Fig. 6: The dynamic response of poly(NIPAM-co-AAc) NPs (120 nm in size): a) schematic of the dynamic measurement; b) the change of relative transmittance with time.

Experimental

Synthesis of (poly(NIPAM-*co*-AAc)) NPs

N-isopropylacrylamide (NIPAM, 98 %), 2-acrylamido-2-methyl-1-propanesulfonic acid (AMPS, 98 %), N,N′-methylenebis(acrylamide) (BIS, ≥99.0 %), sodium dodecyl sulfate (SDS), acrylic acid (AAc, >99 %), and potassium persulfate (99.5 %) were all purchased from Aladdin (Shanghai, China). Ultrapure deionized water was purified by Milli-Q system (Minipore, MA, USA).

To synthesize pNIPAM NPs, first AMPS, BIS, AAc and SDS were all dispersed in ultrapure water through sonication. The solution was then transferred into a 500-mL three-necked round-bottom flask and was heated to 70 °C. After degased for 10 min using nitrogen gas, potassium persulfate was added into the solution to initiate the polymerization reaction. Ultrapure water was also added to the flask to reach a final volume of 300 mL. The reaction was maintained at 70 °C under the nitrogen atmosphere for 6 h.

After polymerization, the solution was cooled down to room temperature and subsequently dialyzed in deionized water for 5 days. During the dialysis process, the water was exchanged every 12 h. After dialysis, the NP samples were further purified using mixed bed ion-exchange resin.

Differential scanning calorimetry (DSC) characterization and solid content measurement

The DSC analysis was carried out using a TA Q200 instrument (New Castle, DE, USA). During the DSC measurement, the temperature was first maintained at 20 °C for 1 min, then raised to 40 °C at a speed of 1 °C/min.

To measure the solid content of the hydrogel NPs synthesized, first ~0.5 mL of hydrogel NP solutions was dropped onto a small piece of aluminum foil and weighted (W1). Then the sample was dried at 120 °C for 1 h and the weight was tested again (W2). The solid content is defined as the ratio of W2 and W1(W2/W1). The measurement was repeated three times to get the average data of solid contents.

Scanning electron microscopy (SEM) and atomic force microscopy (AFM) characterizations

Samples for SEM and AFM characterization were all prepared by spin-coating. The NP solution was first heated to 80 °C for 10 min, then the warm solution was dropped onto the silicon wafer and spun at 350 rpm for 6 s and then 4000 rpm for 30 s.

The SEM images were obtained using a FEI QUANTA 250 SEM system (Hillsboro, OR, USA) and operated at 20 kV. The AFM images were obtained using a Bruker Multimode 8 AFM system.

IR sensitivity measurement

The experimental set up for IR sensitivity measurement is shown in Fig. 7. About 1 mL of poly(NIPAM-*co*-AAc) NP solution was injected into a 5-mL cuvette and illuminated by an IR lamp (TDP CQ-10, Crane Co., Shanghai, China) from the top. The change of transmission spectra of the NP solution was recorded by an optical spectrometer (HR2000+CG, Ocean Optics, USA). The temperature of the sample was measured by a thermocouple that was suspended in the NP solution and was covered with aluminum foil to avoid the influence of IR radiation. To test the response speed of hydrogel NP sample to IR radiation, the sample was exposed to the IR radiation periodically using an optical chopper.

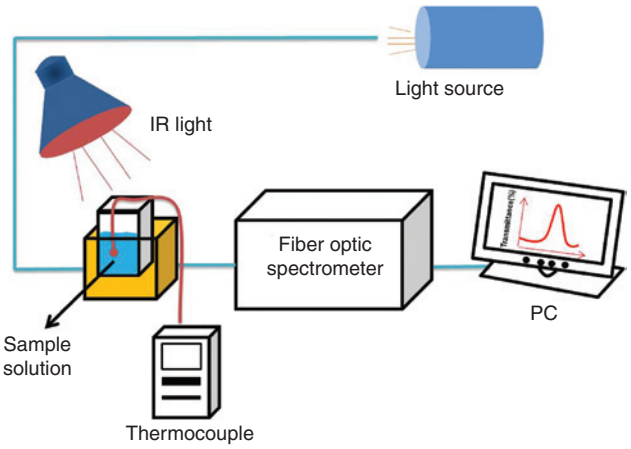

Fig. 7: The schematic of experimental set-up for IR response measurement.

Acknowledgments: The authors greatly thank the Natural Science Foundation of China (Grant No: 91333115), Natural Science Foundation of Shanghai (Grant No: 13ZR1421500), and the Zhi-Yuan Endowed fund from Shanghai Jiao Tong University for the supporting of this work. We also want to thank Hongchen Dong, Kaili Wu, and Xiao Nie for their helpful discussion.

References

[1] C. Downs, T. E. Vandervelde. *Sensors* **13**, 5054 (2013).
[2] A. Rogalski. *Opto-Electron. Rev.* **20**, 279 (2012).
[3] A. Graf, M. Arndt, M. Sauer, G. Gerlach. *Meas. Sci. Technol.* **18**, R59 (2007).
[4] P. Tao, W. Shang, C. Song, Q. Shen, F. Zhang, Z. Luo, N. Yi, D. Zhang, T. Deng. *Adv. Mater.* **27**, 428 (2014).
[5] A. L. Campbell, R. R. Naik, L. Sowards, M. O. Stone. *Micron* **33**, 211 (2002).
[6] J. Hazel, N. Fuchigami, V. Gorbunov, H. Schmitz, M. Stone, V. V. Tsukruk. *Biomacromolecules* **2**, 304 (2001).
[7] H. Schmitz, T. Kahl, H. Soltner, H. Bousack. *Proc. SPIE* **7975**, 797506 (2011).
[8] G. Siebke, P. Holik, S. Schmitz, M. Lacher, S. Steltenkamp. *Proc. SPIE* **8686**, 86860D (2013).
[9] A. D. Pris, Y. Utturkar, C. Surman, W. G. Morris, A. Vert, S. Zalyubovskiy, T. Deng, H. T. Ghiradella, R. A. Potyrailo. *Nat. Photonics* **6**, 195 (2012).
[10] F. Zhang, Q. Shen, X. Shi, S. Li, W. Wang, Z. Luo, G. He, P. Zhang, P. Tao, C. Song, W. Zhang, D. Zhang, T. Deng, W. Shang. *Adv. Mater.* **27**, 1077 (2014).
[11] H. Schmitz, H. Bleckmann, M. Mürtz. *Nature* **386**, 773 (1997).
[12] T. Kahl, H. Bousack, E. S. Schneider, H. Schmitz. *Sensor Rev.* **34**, 123 (2014).
[13] E. O. Gracheva, N. T. Ingolia, Y. M. Kelly, J. F. Cordero-Morales, G. Hollopeter, A. T. Chesler, E. E. Sánchez, J. C. Perez, J. S. Weissman, D. Julius. *Nature* **464**, 1006 (2010).
[14] L. Y. Chu, Y. Li, J. H. Zhu, W. M. Chen. *Angew. Chem. Int. Ed.* **44**, 2124 (2005).
[15] H. Ichikawa, Y. Fukumori. *J. Controlled Release* **63**, 107 (2000).
[16] C. E. Reese, M. E. Baltusavich, J. P. Keim, S. A. Asher. *Anal. Chem.* **73**, 5038 (2001).
[17] J. H. Holtz, J. S. W. Holtz, C. H. Munro, S. A. Asher. *Anal. Chem.* **70**, 780 (1998).
[18] J. M. Weissman, H. B. Sunkara, A. S. Tse, S. A. Asher. *Science* **274**, 959 (1996).
[19] M. Müller, M. Olek, M. Giersig, H. Schmitz. *J. Exp. Biol.* **211**, 2576 (2008).
[20] H. Schmitz, H. Bleckmann. *J. Comp. Physiol. A* **182**, 647 (1998).
[21] M. Keerl, V. Smirnovas, R. Winter, W. Richtering. *Macromolecules* **41**, 6830 (2008).
[22] M. Karg, I. Pastoriza-Santos, J. Pérez-Juste, T. Hellweg, L. M. Liz-Marzán. *Small* **3**, 1222 (2007).
[23] R. A. Potyrailo, H. Ghiradella, A. Vertiatchikh, K. Dovidenko, J. R. Cournoyer, E. Olson. *Nat. Photonics* **1**, 123 (2007).

Supplemental Material: The online version of this article (DOI: 10.1515/pac-2015-0101) offers supplementary material, available to authorized users.